Available online at www.sciencedirect.com
SCIENCE DIRECT
Polymer 46 (2005) 369–382
polymer
www.elsevier.com/locate/polymer

Confined crystallization phenomena in immiscible polymer blends with dispersed micro – and nanometer sized PA6 droplets, part 1: uncompatibilized PS/PA6, (PPE/PS)/PA6 and PPE/PA6 blends

R.T. Tol, V.B.F. Mathot, G. Groeninckx*

Laboratory for Macromolecular Structural Chemistry, Department of Chemistry, Catholic University of Leuven, Celestijnenlaan 200F, B-3001 Heverlee, Belgium

Received 3 April 2004; received in revised form 11 October 2004; accepted 20 October 2004
Available online 2 December 2004

Abstract

In this paper the crystallization behavior of PA6, dispersed as droplets in various immiscible amorphous polymer matrices, is reported. PA6 was melt-mixed at various compositions with PS, (PPE/PS 50/50 wt/wt) and PPE using twin-screw extrusion. The phase morphologies of the obtained blends were analysed using SEM, etching experiments and image analysis. The crystallization behavior of PA6 was investigated by dynamic and isothermal DSC experiments. In case PA6 is dispersed as droplets, fractionated crystallization behavior occurs, characterized by several crystallization events at different, lowered crystallization temperatures. It is found to depend on the blend morphology (size of the droplets) and the thermal history of the samples (heterogeneous nucleation density). The PA6 droplet size distribution is shown to strongly influence the crystallization behavior of the droplets. Vitrification of the matrix appears to cause nucleation in the droplets at the interface. Decreasing the PA6 droplet size results in slower overall crystallization rates.

Keywords: PA6; Droplet crystallization; Blend morphology

1. Introduction

Blending of immiscible polymers is one of the most efficient ways to obtain polymeric materials with specific, beneficial properties. In a lot of these blends a semicrystalline component is dispersed as minor phase into a matrix of another component. In addition, if the semicrystalline polymer is dispersed into confining droplets, effects on the crystallization behavior and semicrystalline structure are to be expected.

Early observations on the effect of dispersion on crystallization were done by Vonnegut for metals [1]. In these experiments the system was subdivided into isolated regions whose number was significantly greater than the number of active heterogeneities. As a result, supercooling for crystallization was found to be much larger than for the undivided sample, which was related to homogeneous nucleation taking place inside the heterogeneity-free droplets. This technique was also applied for polymers by using a 'droplet' technique' in which the polymer was suspended in an inert liquid medium like oil [2–7]. In some cases, the crystallization of these polymer droplets showed a spectrum of activity of heterogeneous nucleation at different degrees of supercooling, which was clearly dependent on thermal history, and as an extreme, possible homogeneous nucleation phenomenon at a very large degree of supercooling [2,5].

Comparable crystallization effects were found for immiscible blends where the dispersed component was crystallizable. Multiple crystallization peaks at different degrees of supercooling were found for several immiscible blend systems, mostly referred to as 'fractionated crystallization' [8–31]. Overviews of fractionated crystallization phenomena in a variety of immiscible polymer blends are given by Frensch et al. [11] and Groeninckx et al. [32].

The following explanation has been proposed for these

* Corresponding author. Tel.: +32 16 327440; fax: +32 16 327990.
E-mail address: gabriel.groeninckx@chem.kuleuven.ac.be (G. Groeninckx).

0032-3861/$ - see front matter © 2004 Elsevier Ltd. All rights reserved.
doi:10.1016/j.polymer.2004.10.085

peculiar crystallization phenomena [11]: when the sample is subdivided in matrix/droplet phases, heterogeneous nucleation of the crystallizable polymer in the droplets is restricted to the volume of the droplet and each droplet will crystallize according to number and type of heterogeneities in it. When the droplet size is small enough, the number of droplets could exceed the number of heterogeneities present that normally promotes crystallization as represented by the bulk crystallization temperature. In such a case, some fraction of the droplets can be nucleated by heterogeneities having a higher specific interfacial energy difference $\Delta\gamma$ than the nuclei active at $T_{c,bulk}$ by which it will crystallize at a lower temperature. Indications for the existence of such less active heterogeneous nuclei were obtained in early crystallization experiments on homopolymers. These experiments indicated an increase of the number of active nuclei at decreasing crystallization temperatures, confirming heterogeneous nucleation triggered by different types of heterogeneities, active at increasing degrees of supercooling [33–36]. Finally, the droplets that do not contain any heterogeneities can undergo homogeneous nucleation at the largest obtainable degree of supercooling. Here, polymer chains have to nucleate on their own. The multiple crystallization peaks thus can be considered to reflect the efficiency spectrum of the several nucleating heterogeneous nuclei available in the dispersed crystallizable polymer phase, and possibly also crystallization triggered by homogeneous nucleation.

The fractionated crystallization phenomenon in immiscible polymer blends has been shown to be strongly dependent on the blend phase morphology [32]. In most cases, only qualitative relations between the size of the dispersed droplets and the fractionated crystallization phenomenon are observed. In addition, many aspects, which are crucial for a fundamental understanding of fractionated crystallization are still unknown. In this first part of a series of papers, we investigate phenomena using uncompatibilized immiscible amorphous/semicrystalline blends with PA6 as the crystallizable polymer.

For uncompatibilized immiscible polymer blends where one polymer is dispersed as droplets, in general quite polydisperse droplet morphologies will be obtained. Only a few authors recognize the importance of the droplet size distribution on the droplet crystallization phenomena [25,29]. In the present work relations between the size distribution of the dispersed crystallizable droplets and the number and intensity of the different DSC crystallization peaks will be investigated. For small, dispersed crystallizable droplets, it can be expected that the interface significantly contributes to the crystallization of these droplets by affecting the nucleation process. Nucleation effects caused by the interface have already been reported for blends were the crystallizable polymer formed the matrix, leading to additional nucleation of the dispersed phase [37]. Barham et al. [7] reported upon shifts in crystallization temperature of PE droplets of more than 40 °C, depending on the type of cover glass used for optical microscopy, clearly indicating the importance of interface effects. Furthermore, it has been observed in immiscible polymer blends that heterogeneous nuclei can migrate from one to the other phase depending on the interfacial tension and the amount of interfacial area [38,39]. In this work interface effects will be investigated for crystallization within droplets using different amorphous /vitrified polymer matrices.

For this study we used immiscible blend systems of PS/PA6, (PPE/PS)/PA6 and PPE/PA6. Varying the matrix phase by changing the PPE and PS fractions allows us to generate strongly different blend morphologies without major changes in interfacial tension of the blend [40]. Furthermore, different physical states of the matrix (vitrified, rubbery, viscous flow) during crystallization can be obtained because the matrix constituting polymers significantly differ in their glass transition temperatures. First an overview of the fractionated crystallization phenomena of PA6 will be given, in which the different effects of the blend morphology (droplet size distribution, number of droplets) will be revealed. Secondly, the effect of different matrices (PS, (PPE/PS) and PPE) on the PA6 crystallization behavior will be investigated.

2. Materials and methods

2.1. Materials

The polymers used in this study are listed in Table 1, together with M_w and T_g and the magnitude of the complex viscosity at 260 °C. Polyamide-6 (PA Akulon K123) was provided by DSM Research, Geleen, The Netherlands. Atactic polystyrene (PS Styron E680) was supplied by DOW Benelux, Terneuzen, The Netherlands. Poly(2,6-dimethyl-1,4-phenelyne ether) (PPE) was supplied General Electric Plastics, Bergen op Zoom, The Netherlands. The miscible polystyrene/polyphenylene-ether (PPE/PS) 50/50 wt/wt mixture was prepared by mixing PPE and PS in a Haake Rheocord 90 twin-screw extruder [41].

Table 1
Molecular characteristics of the blend components used

Materials	M_w [g mol^{-1}]	T_g (DSC) [°C]	η^a at 260 °C 100 rad/s [Pa.s]
PS	190000	102	211
PPE/PS 50/50 wt/wt	54300 / 190000	150	1293
PPE	54300	215	− ($\ggg$1500)
PA6	24000	50	222

[a] Experiments performed on a stress controlled Rheometric Scientific DSR 200 equipped with parallel plate geometry. Viscosity of PPE at 260 °C was too high to be measured.

2.2. Blend preparation

The blends were prepared on a co-rotating twin-screw mini-extruder manufactured by DSM Research. Before processing all materials were dried overnight under vacuum at 80 °C. All blends were mixed at 260 °C for 8 min at a screw speed of 100 rpm, which was sufficient for attaining a steady state morphology. During melt-blending the mixing chamber was saturated with N_2 gas to avoid oxidative degradation. After mixing, the blends were quenched in a mixture of CO_2/isopropanol (−78 °C) in order to freeze the existing phase morphology.

2.3. Morphological characterization via dissolution experiments and SEM

The morphology of the extruded blends was analyzed by means of dissolution experiments. In this manner it could be determined whether the extruded blends displayed a droplet/matrix or a co-continuous phase morphology. A small piece of the sample (about 0.025 cm^3) was immersed in formic acid at room temperature. Formic acid is a solvent for PA6 and a non-solvent for PS, (PPE/PS 50/50), PPE and SMA2. A second piece was put in chloroform at room temperature. Chloroform is a solvent for PS, (PPE/PS 50/50), PPE and SMA2 and a non-solvent for PA6. The complete procedure was repeated twice. With a droplet/matrix morphology, a solvent dissolving the matrix would cause disintegration of the sample, resulting in a milky suspension. The solvent for the droplet phase will just extract that phase, leaving the matrix intact. In a co-continuous system, neither of the solvents would cause a complete disintegration of the blend. The blends were assumed to be co-continuous when the samples were still self-supporting after soaking them in formic acid and chloroform.

The morphology of the blends has also been characterized by scanning electron microscopy (SEM) on a Philips XL20. An extruded polymer strand was first broken in liquid nitrogen to obtain a fracture surface perpendicular to the extrusion direction. A Leica Ultracut UCT cryo-microtome, equipped with a Leica EM FCS cryo unit, at a sample temperature of −100 °C was used to smoothen the fractured surface. Subsequently, the samples were exposed to either formic acid or to chloroform (16 and 40 h respectively) to remove one phase. The etched surface was dried under vacuum and then coated with a conductive gold layer before SEM analysis. The SEM photographs used for image analysis (section 2.4) were obtained after subjecting the samples to the same thermal program as used in dynamic crystallization experiments with DSC (section 2.5).

2.4. Image analysis

Image analysis on the obtained SEM micrographs was performed using Leica Qwin image analysis software. The morphological parameters of the blends were quantified as follows. For the systems with a droplet/matrix structure, the average sizes and the size distribution of the dispersed droplets were determined. About six SEM photographs (each containing about 150–300 droplets) were analysed for each blend. The number average droplet diameter (D_n), volume average diameter (D_v) and the polydispersity (P) were calculated from:

$$D_n = \frac{\sum_i n_i d_i}{\sum_i n_i} \tag{1}$$

$$D_v = \frac{\sum_i n_i d_i^4}{\sum_i n_i d_i^3} \tag{2}$$

Polydispersity: $P = D_v/D_n$ with n_i the number of droplets having diameter d_i.

The characteristic diameters are given as seen in SEM and were not corrected for the fact that not all droplets were cut at their largest cross-section. The total number of droplets per unit volume (dispersed) polymer was calculated from:

$$N_n = \frac{X}{(\pi/6(D_n)^3)} \tag{3}$$

$$N_v = \frac{X}{(\pi/6(D_v)^3)} \tag{4}$$

with: N_n: total number of droplets per unit volume based on D_n, N_v: total number of droplets per unit volume based on D_v, X: volume fraction of dispersed phase in the blend.

Number and volume droplet size distributions were constructed by dividing each dataset of droplet sizes into a number of size intervals of equal length. The length of this interval was selected in such a way that for the number distribution as well as for the volume distribution statistically reliable profiles could be constructed. For obtaining the number distribution, the number of droplets in each size interval was counted and divided by the total amount of droplets. For the volume distribution, the volume of the droplets was counted for each size interval and divided by the total volume of the droplets.

2.5. Thermal analysis

2.5.1. Dynamic and isothermal crystallization experiments

Dynamic and isothermal DSC measurements were performed using a Perkin Elmer Pyris 1. The nitrogen flow-rate was 20 ml/min. Temperature and enthalpy calibrations were performed with indium (T_m = 156.6 °C) and tin (T_m = 231.88 °C) at a heating rate of 10 K/min. Furnace calibration was performed between 0 and 290 °C. For the dynamic measurements the samples were first heated at a rate of 40 K/min to a melt temperature of 260 °C, and kept there for 3 min in order to erase all thermal history. In one experiment this isothermal time was extended to 60 min.

Then, the samples were cooled at 10 K/min to 25 °C. Subsequent melting scans were performed at a rate of 10 K/min. Sample masses of about 5 mg were used in case of scan rates of 10 K/min. Weighing was done using an AND Hm-202 balance with an accuracy of 0.01 mg. Sample masses were adjusted according to the applied cooling rate (approximately 0.5 mg for 100 K/min, 5 mg for 10 K/min; ~10 mg for 1 K/min and ~20 mg for 0.1 K/min). DSC curves were corrected for instrumental curvature by subtracting empty-pan curves, measured using identical thermal histories at the beginning and end of each day.

For the isothermal crystallization measurements the sample was heated at a rate of 40 K/min to a melt temperature of 260 °C, and kept there for 3 min, similar to the dynamic experiments. In the second step the sample was cooled down to the isothermal crystallization temperature T_{iso} at a rate of 10 K/min, followed by an isothermal period long enough to complete measurable crystallization of the material at the particular isothermal temperature. Subsequent melting after isothermal crystallization was performed at a heating rate of 10 K/min. A normal calibration set-up at 10 K/min heating rate was used for calibration but the isothermal temperature was each time set corresponding to the real sample (sensor) temperature (instead of the DSC program temperature). The crystallization half time was determined by calculating the time to reach 50% of the total area under the isothermal peak as a function of time.

2.5.2. Self-nucleation experiments

Self-nucleation experiments were also performed using the Pyris 1 DSC. With this method the nucleation density is increased enormously by heating up the material within the self-nucleation regimes where small crystal fragments are still present in the melt [42]. These tiny regions of a high degree of order, often stabilized by foreign substrates, may persist in the melt and will act as predetermined nuclei for recrystallization upon cooling and can cause the nucleation process to start at higher temperatures than would normally be the case. Mathot [43] showed that temperatures within the self-nucleation regimes prior to crystallization increased the crystallization temperature for various nylons (PA6, PA6.6 and PA4.6). Reported heterogeneous nucleation densities vary from ~10^6 nuclei/cm^3 after crystallization from the completely molten state to typically 10^{10}–10^{12} nuclei/cm^3 after crystallization from the self-nucleation region [44]. Fillon et al. [44–46] showed the applicability of dynamic DSC for studying self-nucleation in polymer melts. Müller et al. [22,24,26,28] recently showed in a number of papers the particular use of a self-nucleation technique for investigating fractionated crystallization in immiscible polymer blends.

The following procedure was applied in this investigation:

Step 1) Erasing thermal history and creating a initial standard state. The samples were first heated to 260 °C at 40 K/min, and kept there for a 3 min isothermal period. Subsequently, the samples were cooled to room temperature at a cooling rate of 10 K/min.

Step 2) Heating to T_s (Self-nucleation temperature), situated between 220–260 °C, at a heating rate of 10 K/min. If T_s is 260 °C or higher, the sample is said to be in domain I, where complete melting is realized. When T_s is high enough to melt the material almost completely, but low enough to leave small crystal fragments capable of acting as self-nuclei, this is domain II, the self-nucleation region. When T_s is too low, only part of the crystals will be melted, and quite some remaining crystals will be annealed at T_s. This is domain III, giving rise to both self-nucleation and annealing.

Step 3) Isothermal conditioning at T_s during 3 min.

Step 4) Crystallization at a cooling rate of 10 K/min from T_s to room temperature.

Step 5) Melting after crystallization at a heating rate of 10 K/min.

The self-nucleation runs were performed each time on a fresh sample for every temperature T_s used.

2.6. Calculation of the number of heterogeneities active at $T_{c,bulk}$

For the calculation of the number of heterogeneities it is assumed that the distribution of heterogeneities over the droplet population follows a Poisson distribution, analogue to the approximation of Pound and LaMer for the distribution of heterogeneities for monodisperse tin droplets [47]. Considering a large number of small polymer droplets, each having a volume V_D, the fraction of droplets that contain exactly z heterogeneities of type i that can nucleate the polymer can then be given by [47]:

$$f_z^i = [(M^i V_D)^z / z!]\exp(-M^i V_D) \quad (5)$$

where M^i is the concentration of heterogeneities of type i, and $M_i V_D$ is the mean number of heterogeneities per droplet with volume V_D.

The fraction of droplets, which contain at least one heterogeneity of type i is given by:

$$f_{z>0}^i = 1 - \exp(-M^i V_D) \quad (6)$$

or:

$$M^i = -[\ln(1 - f_{z>0}^i)]/V_D \quad (7)$$

This fraction can be calculated from the relative partial area of each crystallization exotherm during cooling in the DSC. On the assumption that one nucleus is sufficient to crystallize the whole droplet, calculations can be done with respect to the concentration of the respective heterogeneities, if the mean size of the droplets is known [11]. So

for $i=1$, corresponding to the type of nuclei active at $T_{c\,(bulk)}$, one can calculate:

$$M^1 = -[\ln(1 - f^1_{z>0})]/V_D \quad (8)$$

$$\text{in which} = \frac{\Delta h_c \text{bulk}}{\Delta h_c \text{total}} \quad (9)$$

2.7. Transmission electron microscopy (TEM)

TEM micrographs of extruded PA6 (cooled at the air from the melt) were made on a Philips CM10, operating at 80 kV. Ultrathin sections were prepared on a Leica Ultracut UCT microtome, equipped with a Leica EM FCS cryo unit. The samples were trimmed with iron trimming knifes to trapezoidal shaped faces. Ultrathin sections (75 nm or less) were microtomed from these faces with a diamond knife (Drukker International) at a sample temperature of −90 °C and with a knife temperature of −75 °C. The microtomed sections were collected in a water/dimethylsulfoxide (50/50) filled boat, attached to the diamond knife. The sections were collected out of the boat on copper TEM grids (square, 300 mesh) and dried completely on filter paper. The cuts on the grid have been selectively stained with phosphotungstic acid for 60 min to increase contrast between the phases.

3. Results and discussion

3.1. Crystallization behavior of PA6 in PS/PA6 and (PPE/PS)/PA6 blends, as determined by DSC cooling experiments

The dynamic crystallization behavior of PA6 in PS/PA6, and in (PPE/PS)/PA6 blends with a (PPE/PS) ratio of 50/50 wt/wt, was investigated as a function of the concentration of PA6 in the blends. In Fig. 1 the DSC cooling curves are shown for the two blend series as a function of the blend composition. Fig. 2 shows enlargements of the low intensity DSC crystallization peaks of PA6 in the (PPE/PS)/PA6 blends.

The PA6 crystallization in these two blend series turns out to be strongly dependent on the blend composition. A detailed analysis of the PS/PA6 and (PPE/PS)/PA6 blend morphology as a function of the blend composition was reported recently [48]; these data are summarized in Table 2. It can be seen that the droplet size decreases with decreasing amounts of PA6 in the blend, as the chance for coalescence of PA6 droplets decreases with decreasing concentration of the dispersed phase. Temperatures and heats of crystallization and heats of melting as determined by DSC are also given in Table 2. For blend compositions where PA6 constitutes the matrix, no significant changes in crystallization behavior are observed. For lower concentrations of PA6, however, in both blend systems a

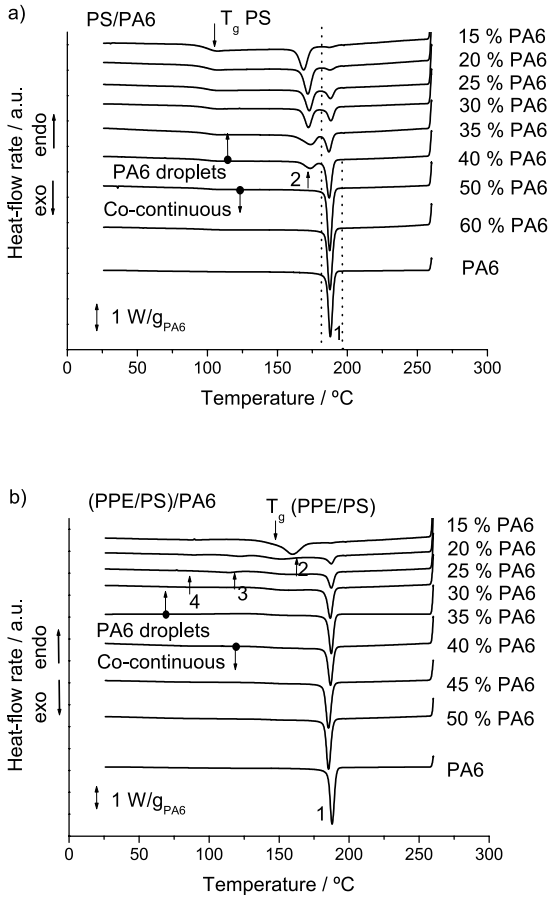

Fig. 1. DSC cooling curves at 10 K/min for a) PS/PA6 and b) (PPE/PS)/PA6 blend compositions.

fractionated crystallization behavior is observed, leading to multiple crystallization peaks at different degrees of supercooling. The occurrence of fractionated crystallization is clearly connected with the blend morphologies where PA6 is dispersed as droplets inside the matrix of PS or (PPE/PS). When the PA6 droplet size is relatively big, most of the PA6 droplets crystallize around the PA6 bulk temperature (188 °C), denoted by 1 in the figures. When

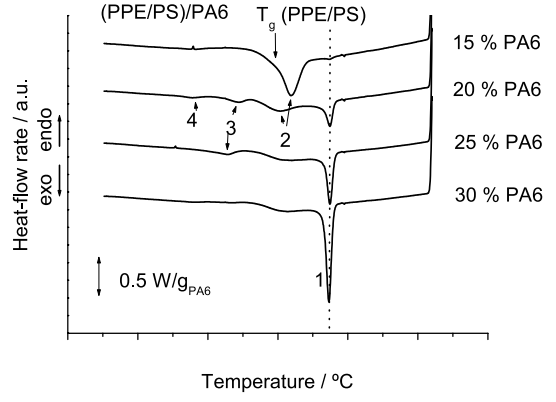

Fig. 2. DSC cooling curves for a number of (PPE/PS)/PA6 blend compositions with PA6 droplets.

Table 2
Morphological and thermal properties of PS/PA6 and (PPE/PS)/PA6 blend compositions

Blend system	Wt% PA6	D_n PA6 [μm]	(D_v/D_n) [−]	N_n [cm^{-3}]	$T_{c,peak}$ [°C]				Δh_c [J/g$_{PA6}$]				Δh_m [J/g$_{PA6}$]
					1	2	3	4	1	2	3	4	
PA6	100	–	–	–	189	–	–	–	77	–	–	–	81
PS/PA6	15	1.42	1.6	1×10^{11}	188	169	–	–	2	51	–	–	53
	20	1.77	1.5	6.8×10^{10}	188	172	–	–	4	48	–	–	55
	25	2.1	2.4	5.2×10^{10}	188	173	–	–	12	42	–	–	55
	30	2.8	2.7	2.6×10^{10}	188	172	–	–	23	37	–	–	62
	35	3.7	2.6	1.2×10^{10}	187	174	–	–	32	33	–	–	65
	40	7.0[a]	4.8	2.2×10^{9}	187	173	–	–	56	14	–	–	68
	45	- (Co-cont.)	–	–	190	–	–	–	71	–	–	–	77
	50	- (Co-cont)	–	–	187	–	–	–	74	–	–	–	75
	60	Matrix PA6	–	–	187	–	–	–	76	–	–	–	79
(PPE/PS) / PA6	15	0.35	3.1	6.7×10^{12}	187	162	–	89	1	36[b]	–	<1	49
	20	0.57[c]	9.3	2.0×10^{12}	187	~160[b]	122	89	13	14[b]	3	1	54
	25	0.61[c]	12.4	2.1×10^{12}	187	~160[b]	113	–	22	12[b]	5	–	60
	30	4.6[a]	3.9	5.9×10^{9}	187	~160[b]	117	90	40	18[b]	<1	<1	63
	35	5.1[a]	4.7	5.0×10^{9}	187	~160[b]	110	88	49	6[b]	<1	<1	≥65[d]
	40	- (Co-cont)	–	–	187	~160[b]	–	88	51	<1	–	2	>61[d]
	45	- (Co-cont)	–	–	186	–	–	–	62	–	–	–	>74[d]
	50	Matrix PA6	–	–	186	–	–	–	63	–	–	–	>71[d]

[a] Break-up of initial co-continuous morphology into a droplet/matrix morphology during DSC treatment prior to crystallization.
[b] These crystallization peaks could not be determined accurately due to overlap of the peaks with the glass transition of (PPE/PS) (T_g ~150 °C). Peak intensities as given were determined from the relative increase of the melting enthalpy before and after crystallizing this peak and by assuming that the crystals formed in this temperature region did not show extensive reorganization or recrystallization during heating.
[c] Break-up of co-continuous morphology into a morphology with bimodal droplet size distribution during DSC treatment prior to crystallization [48].
[d] These data could be a little underestimated because of overlap of the onset of the melting peak with the glass transition of (PPE/PS).

the phase morphology becomes finer and the number of PA6 droplets per unit volume increases, a significant portion of the droplets crystallizes at a higher degree of supercooling. This is thought to be caused by the heterogeneous nucleation of nuclei of different activity, having a higher interfacial energy difference between nucleus and melt. Therefore these need an increased supercooling to become active. The relative intensity of the related crystallization peaks is higher the finer the blend morphology. This fractionated crystallization effect however, is clearly different for the two blend systems. For the PS/PA6 blends the second (lower temperature) crystallization peak (denoted by 2) can be found between 168 and 177 °C, about 10–15 °C lower than the bulk temperature. The second crystallization peak for the (PPE/PS)/PA6 blends is situated around 160 °C, which partly overlaps with the T_g of the (PPE/PS 50/50 wt/wt) component, which is about 150 °C. Interestingly, a third crystallization peak is observed for some (PPE/PS)/PA6 blend compositions at temperatures between 110 and 120 °C, denoted by 3. Finally, a small part of the (PPE/PS)/PA6 blends crystallizes at about 90 °C, denoted by 4. For the (PPE/PS) blends, a part of the material thus crystallizes below the vitrification temperature of the matrix phase (150 °C). The crystallization peak at very large degree of supercooling is possibly related to homogeneous nucleation of PA6, when all heterogeneous nuclei have been exhausted.

These results agree qualitatively with fractionated crystallization peaks reported for PA6 in other works, although it is obvious that a direct comparison can be somewhat ambiguous, because the type of nuclei may vary in different polymer grades. Tang et al. [18] observed a second peak at about 155–165 °C in EPDM/PA6 blends. Ikkala et al. [17] report a crystallization peak of PA6 at about 85 °C in SEBS-g-MAH /PA6 blends, which was explained by homogeneous nucleation of PA6. Dedecker and Groeninckx [49] found PA6 crystallization peaks at 160 °C and 90–100 °C for reactively compatibilized PMMA/PA6 blends. Sanchez et al. [31] observed crystallization peaks of PA6 in ULDPE-g-DEM (Diethylmaleate) /PA6 blends at 158 °C and around 105–115 °C.

In Fig. 3 the effect of cooling rate on the crystallization temperatures of PA6 in PS/PA6 75/25 and (PPE/PS)/PA6 75/25 blends is presented. As expected, lowering the cooling rate shifts the crystallization peaks of PA6 and the crystallization bulk peaks for the blends to higher temperatures. Fig. 3 also shows that the position of the lower crystallization peak (2) is clearly less sensitive to changes in cooling rate. This even could lead to overlap of the bulk crystallization peak with the lower temperature peak upon very fast cooling rates, as can be seen in Fig. 4. The reason for this observation is most likely related to a change in heterogeneous nucleation kinetics, as is discussed in more detail in another paper [50]. The number of fractionated crystallization peaks was found to be independent of the applied cooling rate when it was varied between

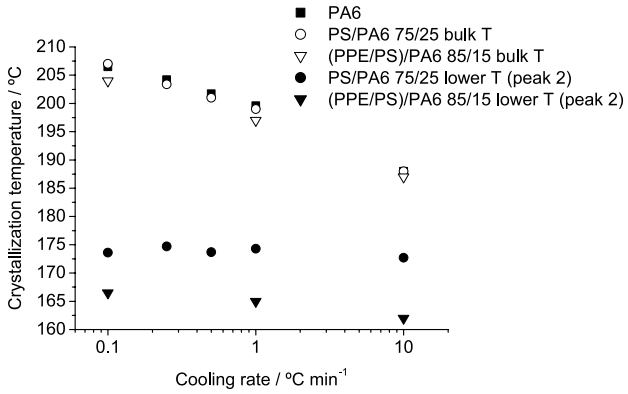

Fig. 3. Peak crystallization temperatures of bulk and fractionated crystallization peaks for PA6, PS/PA6 75/25 and (PPE/PS)/PA6 85/15 blends as function of the DSC cooling rate.

10 and 0.1 K/min. The relative intensity of the crystallization peaks too was almost unchanged upon changing the cooling rate. In Fig. 3 can also be seen that the lower crystallization temperature of the (PPE/PS)/PA6 85/15 blend is significantly lower than the lower temperature peak of the PS/PA6 blend, independent of the cooling rate (160–165 °C, compared to 170–175 °C). This is in line with the much smaller PA6 droplet size of the (PPE/PS)/PA6 85/15 blend compared to the PS/PA6 75/25 blend (see Table 2). The lower crystallization peak of the PS/PA6 series is found to decrease upon blending lower amounts of PA6, which corresponds to a decrease of the crystallization peak with smaller PA6 droplets, see Table 2. Similar reductions of T_c were reported by Everaert et al. [29] for $T_{c,bulk}$, again related to the decrease in droplet or domain size. Due to the effect of volume limitation, the overall crystallization rate in droplets is reduced [50,51] which leads to a decrease in the observed crystallization temperature. Even the PA6 bulk crystallization peak temperature is somewhat decreased (2–3 °C) upon blending, which decrease slightly depends on the type of matrix phase (PS or (PPE/PS). Migration of nuclei during melt-blending can also shift the observed T_c, but the reported shifts are much smaller (~1 °C) [38]. Additional experiments on the effect of the droplet size on the PA6 crystallization rate will be presented in 3.2.2.

3.2. Effect of thermal history on fractionated crystallization behavior

3.2.1. Changing blend morphologies in the melt

The results presented above show that the occurrence of fractionated crystallization is connected to the presence of dispersed PA6 droplets. In general, a co-continuous morphology is therefore expected to give rise to crystallization around the bulk temperature, because for such a morphology, nucleation can trigger crystal growth within the total volume occupied by crystallizable polymer chains.

One would expect that the phenomenon of fractionated crystallization could possibly be a useful tool to deduce

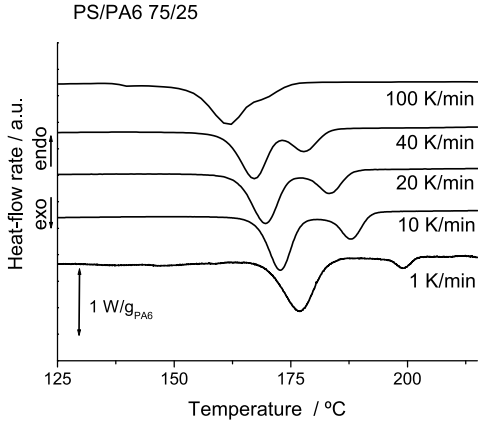

Fig. 4. DSC cooling curves of a PS/PA6 75/25 blend at different cooling rates.

whether a droplet/matrix morphology has been obtained. Such a way of characterization, however, has to be applied with care. First of all, the crystallization behavior of the blend, using DSC, should always be compared with the morphology obtained after a similar thermal history as applied by DSC. This was clearly evident from the crystallization of the present PS/PA6 and (PPE/PS)/PA6 blends, where quite a number of blend compositions, which were clearly identified as being co-continuous directly after extrusion, displayed fractionated crystallization behavior upon cooling in the DSC. This unexpected result was found to be caused by a significant decrease in co-continuity after applying the DSC treatment. Obviously, this treatment—including time spent at high temperatures—results in partly or full break-up of the co-continuous morphology to a dispersed/matrix type of morphology, which is indicated in Table 2. A description of the morphology and stability of these co-continuous morphologies can be found in a previous paper [48].

In addition, a closer observation of the morphological data reveals that multiple crystallization already does take place inside the co-continuous region for the (PPE/PS) /PA6 blends having 40% PA6. Previous results showed that a significant fraction of small inclusions of PA6 within the co-continuous (PPE/PS) phase was found [48]. It is very likely that fractionated crystallization is caused by these very small PA6 small inclusions, reflected by the crystallization peaks at 160 and 90 °C. For blends with PS in the co-continuous phase no small inclusions were found. As expected, for the latter blend system, fractionated crystallization only takes place in case PA6 is fully dispersed as droplets.

Another experiment that indicates the strong effect of thermal history on the droplet crystallization behavior in immiscible polymer blends is presented in Fig. 5. Significant changes in the peaks related to fractionated crystallization of the (PPE/PS) PA6 and PS/PA6 blends can be observed upon changing the residence time in the melt in the DSC apparatus before cooling to room temperature. For the PS/PA6 75/25 blend, the amount of bulk crystallization increases at the expense of fractionated crystallization at 170 °C. For the (PPE/PS)/PA6 75/25 blend, the heating treatment causes an increase of the second crystallization peak, at the expense of the peaks at lower temperatures. The number of peaks is reduced from three to two. These effects can be explained by the significant increase of the droplet sizes as a result of coalescence caused by the increased time in the melt. The bigger the droplet size, the greater the chance that the PA6 chains within the droplets will crystallize by a nucleus active at $T_{c,bulk}$, resulting in less fractionated crystallization. The phenomena seen are not caused by an increase of the nucleation density as related to the thermal treatment, because an increased time in the melt generally leads to destruction of remaining nuclei, which survived earlier thermal treatment. So, it would stimulate fractionated crystallization, contrary to what is seen.

3.2.2. Self-nucleation experiments

In Fig. 6, the crystallization and melting behavior of PA6, and PS/PA6 75/25 and (PPE/PS)/PA6 75/25 blends is presented for different premelting temperatures. The cooling and melting curves of PA6 after premelting to T_s, clearly show the different effects upon changing the premelting temperature. When T_s is high enough (for this PA6: $\geq$240 °C) the crystallization temperature is unaffected by T_s (domain I crystallization). The subsequent melting at 10 K/min of PA6 exhibits a double melting behavior, which appears to be caused by recrystallization (see [52]). When T_s is lowered below 240 °C, the self-nucleation domain is reached (domain II), where the amount of nuclei strongly increases upon lowering the self-nucleation temperature T_s. It can be seen that the crystallization temperature as well as the crystallization and melting enthalpy after crystallization slightly increase in this region, as a result of the increased nucleation density. Additionally, a third melting peak at about 205 °C is observed for PA6 after self-nucleation (domain II), which cannot be easily explained.

Finally, upon further lowering the temperature, the self-nucleation and annealing domain is reached (domain

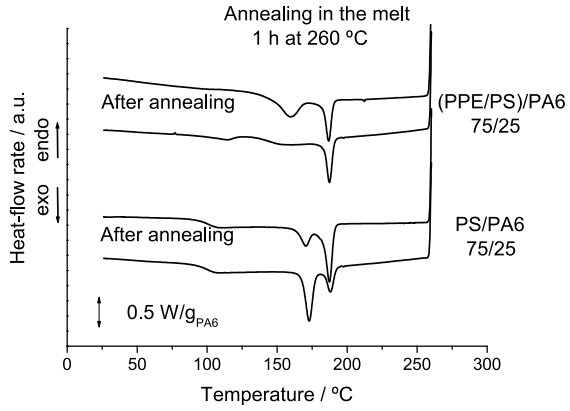

Fig. 5. DSC cooling curves at 10 K/min of PS/PA6 75/25 and (PPE/PS)/PA6 75/25 blends before and after annealing in the melt for 1 h in the DSC.

III), where large crystal parts remain unmolten and can perfection themselves. As a result a higher melting point of 225 °C is found for these crystals (peak nr. 4 in melting plot of Fig. 6(a)). This domain can be identified by a decrease of the crystallization enthalpy, because the unmolten material will not crystallize in the subsequent cooling run. Note that crystallization starts almost immediately upon cooling from the lowest premelting temperature of 221 °C.

The crystallization behavior of the PA6 droplets in the PA6/PS 75/25 and (PPE/PS)/PA6 75/25 blends changes strongly upon self-nucleation ($T_s \leq 240$ °C). A clear reduction of the area under the second, lower crystallization temperature peak is observed upon lowering T_s for PS/PA6 75/25, accompanied by the simultaneous increase of the bulk crystallization peak

In Fig. 7 the crystallization temperature and the melting enthalpy after crystallization are plotted for different premelting temperatures T_s for the PS/PA6 75/25 blend. The increase in crystallization bulk temperature and the increase in melting enthalpy for crystallization in domain II (self-nucleation) can clearly be observed (increased nucleation density). At a premelting temperature of about 225 °C no fractionated crystallization can be observed anymore for this blend in the subsequent cooling run. The same results

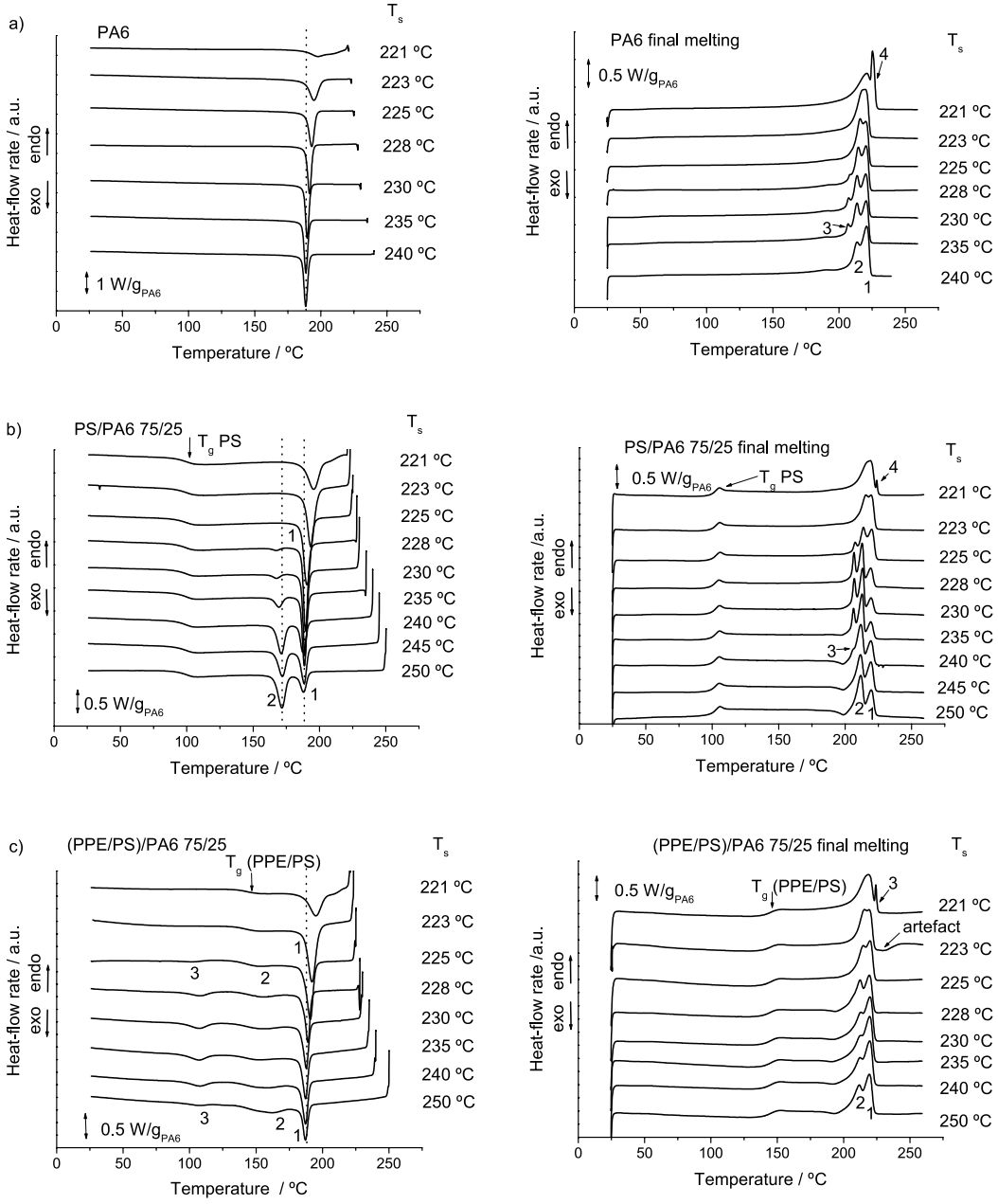

Fig. 6. DSC cooling and melting curves at 10 K/min after premelting to the indicated temperatures for the PA6 (a) a PS/PA6 75/25 blend (b) and a (PPE/PS)/PA6 75/25 blend (c).

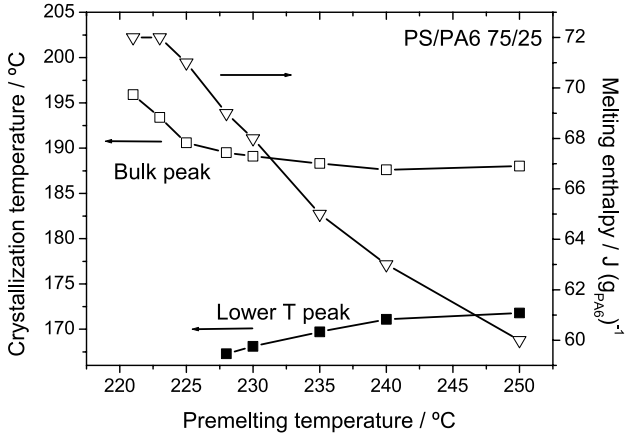

Fig. 7. Evolution of crystallization temperature and melting enthalpy as a function of thepremelting temperature for a PS/PA6 75/25 blend.

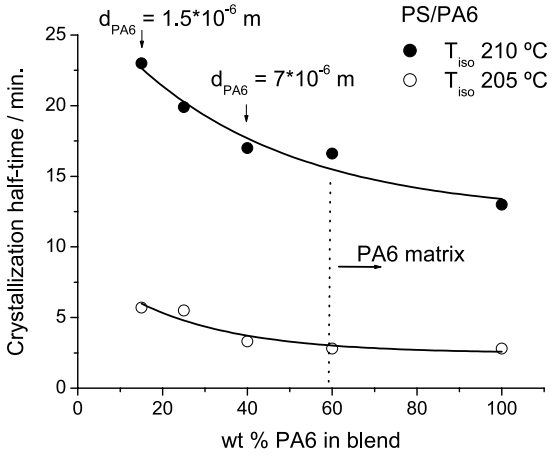

Fig. 8. Crystallization half-times at 210 and 205 °C for different PS/PA6 blend compositions after premelting to T_s=223 °C.

are found for (PPE/PS)/PA6 75/25. Note also that the PA6 crystals all melt at the same melting peak (~220 °C), whereas they were formed at different crystallization temperatures. Interestingly, it is observed from Fig. 7 that the lower temperature peak shifts to lower crystallization temperatures upon self-nucleation. The PS/PA6 75/25 peak decreases gradually from 173 to 167 °C upon increasing nucleation density. Most likely, first the most active heterogeneous nuclei are activated by the self-nucleation substrates, leaving lesser active nuclei, crystallizing at somewhat lower temperature. These self-nucleation experiments provide an efficient way to prove that the cause of the fractionated crystallization is the lack of active heterogeneities in the PA6 droplets, and that fractionated crystallization phenomena can be suppressed completely if enough nuclei are introduced [22].

Fig. 8 shows the crystallization half-time as a function of the blend composition for the PS/PA6 blend for two different isothermal crystallization temperatures after self-nucleation at 223 °C. The inverse of the crystallization half-time in isothermal crystallization can be taken as a measure of the overall crystallization rate. As was shown before, premelting to 223 °C effectively suppresses all fractionated crystallization for this blend system. For these self-nucleated blends, the complete droplet size distribution now crystallizes around the same temperature. In this way, the overall crystallization rate can be used to measure the direct effect of the droplet size on the crystallization. A clear increase of the crystallization half time is observed upon decreasing the PA6 content of the blends, which corresponds to a decrease of the PA6 droplet size. This result thus indicates that small droplet sizes can slow down the crystallization kinetics (leading to lower T_c), confirming the discussion at Fig. 3, where the decrease of $T_c(2)$ was related to the droplet size. It can be anticipated that the number of self-nuclei generated can depend on the level of crystallinity prior to melting to T_s. An increase in the number of generated self-nuclei can influence the observed crystallization half-time plotted in Fig. 8. For the presented blends, however, the quantity of crystals before the final melting attains an almost similar value for the presented PS/PA6 blends, due to cold crystallization prior to melting [52], and thus cannot explain the increase in crystallization half-time.

3.3. Quantification of the fractionated crystallization phenomena: heterogeneous nucleation density vs. number of dispersed droplets per unit volume

3.3.1. Effect of the droplet size distribution and calculation of the heterogeneous nucleation density

The fractionated crystallization phenomenon can be interpreted as a statistical problem, critically determined by the number of nuclei that can develop during cooling and the total amount of droplets. One would expect a direct relation between the degree of fractionated crystallization and the number of droplets per unit volume when the total nucleation density developed during cooling remains constant (identical thermal histories, no nucleating agents etc.). Fig. 9 shows the strong relation between fractionated crystallization and the phase morphology. For this plot the degree of fractionated crystallization was calculated by dividing the sum of crystallization enthalpies -as calculated from all crystallization peak areas at supercoolings lower than the PA6 bulk peak -by the total crystallization enthalpy obtained with DSC (note that the degree of fractionated crystallization determined in this way equals $(1-f^1_{z>0})$ in Eq. (8)). The number of droplets in this figure was calculated according to Eq. (3), using a number average droplet diameter. Alternatively, the degree of fractionated crystallization can be plotted as a function of the number average droplet size, which yields the same general behavior as when plotting the number of droplets per unit volume.

Starting from a number of droplets of about 10^9 per cm^3, the degree of fractionated crystallization increases with

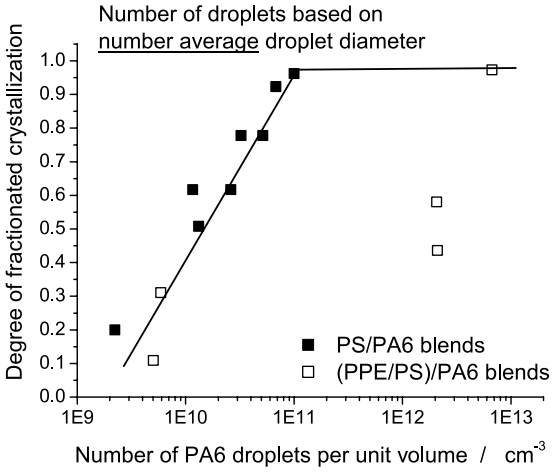

Fig. 9. Degree of fractionated crystallization as a function of the number of PA6 droplets per cm^3, calculated via the number average droplet diameter (Eq. (3)), for PS/PA6 and (PPE/PS)/PA6 blend compositions.

increasing number of droplets until it finally reaches a plateau value close to 100% fractionated crystallization. It can, however, also be seen that the (PPE/PS)/PA6 blend series clearly deviates from the PS/PA6 data. These two blend series differ in their polydispersity of droplet sizes. In Fig. 10 the volume and number droplet size distributions of some PS/PA6 and (PPE/PS)/PA6 blend compositions are represented. In these graphs the volume and number fraction per interval is plotted, using a constant interval width. The number and volume average droplet size values, as determined by Eqs. (1) and (2), are included in the graphs. Using a volume average, the bigger sized droplets are more accentuated, leading to $D_{v(average)} > D_{n(average)}$, which can clearly seen in Fig. 10.

For the PS/PA6 75/25 and PS/PA6 60/40 blends, the volume data are represented by a single Gaussian curve. For the (PPE/PS)/PA6 75/25 and 80/20 compositions, however, which were initially co-continuous but show break-up during the DSC thermal treatment into a droplet/matrix morphology, a different volume distribution profile has to be plotted. The SEM photographs of these two blend compositions revealed a multimodal droplet size distribution with a group of relatively large sized droplets and a group of small droplets, leading to a very large polydispersity factor (see Table 2). For these blends, several peaks can be observed in the volume distribution, indicated

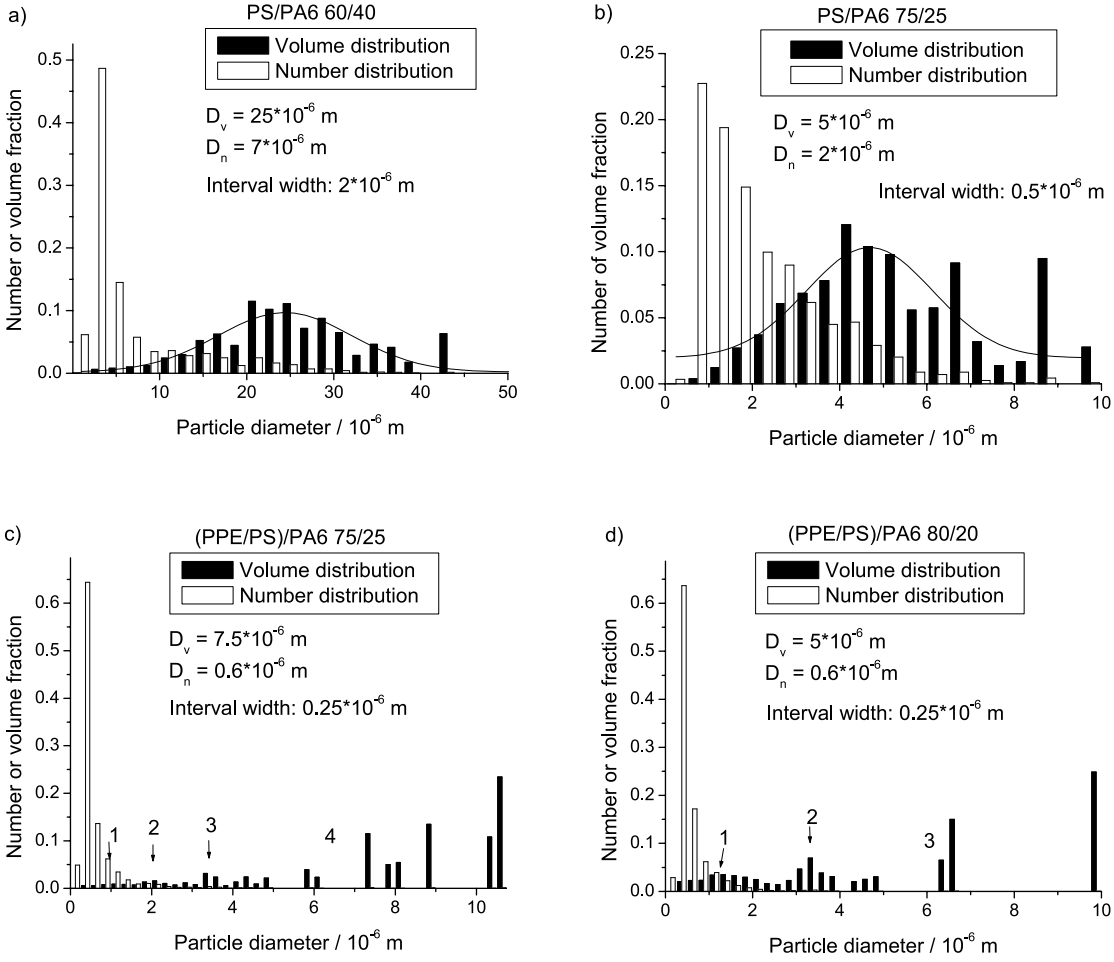

Fig. 10. Number and volume distributions of PA6 droplet diameter for various blends (a) PS/PA6 60/40, (b) PS/PA6 75/25, (c) (PPE/PS)/PA6 75/25 and (d) (PPE/PS)/PA6 80/20.

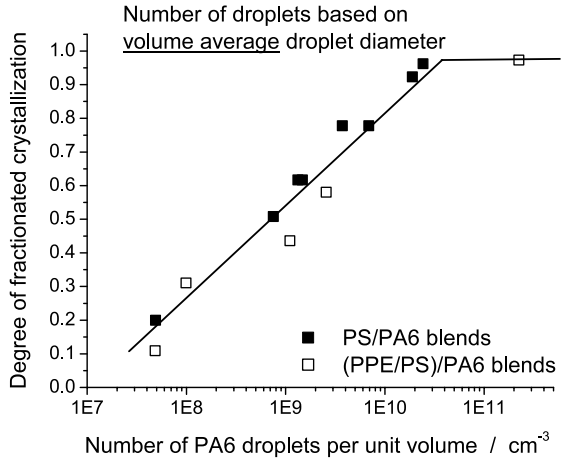

Fig. 11. Degree of fractionated crystallization for PS/PA6 and (PPE/PS)/PA6 blend compositions as a function of (a) number of PA6 droplets per cm^3, calculated via the volume average droplet diameter (Eq. (4)).

with numbers. Interesting enough these two blend morphologies correspond to the two very dissimilar points at the right hand side of Fig. 9.

In Fig. 11 the degree of fractionated crystallization is again plotted versus the number of droplets per cm^3, but now the number of droplets is calculated using a volume average droplet diameter, as given in Eq. (4). It is quite clear that this plot shows a much better agreement of the (PPE/PS)/PA6 data and both blend series can now be fitted using the same line. The explanation for this is likely caused by the underestimation of the degree of fractionated crystallization in case of a broad droplet size distribution: for a blend with a bimodal droplet size distribution consisting of very big droplets and very small ones, the big droplets will most likely contain enough nuclei to induce nucleation at the highest crystallization temperature (bulk nucleation), whereas the very small droplets have much more chance to be free from heterogeneous nuclei. As the intensity of the crystallization peaks is determined by the amount of crystallizable material, which is related to the volume of the droplet, a relative small number of big droplets can already have a big effect on the observed degree of fractionated crystallization. This thus easily leads to an underestimation of the degree of fractionated crystallization when applying the number average droplet size for determining the number of droplets, as shown in Fig. 9.

The data plotted above can be used to determine the heterogeneous nucleation density by determining the relative fraction of droplets crystallizing at $T_c < T_{c,bulk}$ via calculation of the DSC crystallization enthalpies and using Eqs. (8) and (9). For this estimation we assume that the value for $\Delta h_{100\%}$ is similar for the PA6 crystals formed at different temperatures. Using for V_D the volume average droplet diameter yields values for the heterogeneous nucleation density at $T_{c,bulk}$ between 10^9–10^{10} nuclei/cm^3 for the blend compositions given in Fig. 11. From TEM photographs of extruded PA6 cooled from the melt in the air, the average diameter of the PA6 spherulites was determined at about 5 μm (an example is given in Fig. 12). Assuming a close packing of spherical spherulites occupying 72% of the total volume, the number of spherulites per cm^3 was estimated to be $\sim 1.5 \times 10^{10}$ nuclei/cm^3. This value for the nucleation density can be nicely compared to the estimation using the degree of fractionated crystallization. Eqs. (5)–(9) are strictly valid for monodispers droplet distributions, but thus seem to give a quite reasonable description of the fractionated crystallization phenomena for quite polydisperse droplet distributions also. However, the approach has got its limitations. The number of crystallization peaks namely seems to depend on the droplet size distribution. Typically, the two blends with the bimodal droplet distribution exhibit extra crystallization peaks compared to the blends with a single distribution profile. This can possibly be explained by the fact that the chance for obtaining crystallization nucleated by other types of nuclei is increased for broad distributions. The different peaks can be seen to correspond to the crystallization of groups of droplets of a certain droplet size interval, containing a specific type of nuclei. In this case, a Poisson distribution over a total average droplet size does not work, and separate distributions have to be calculated for each average droplet size interval. An interesting approach to proof this would be via fractionating of the separate droplet size intervals and measuring each fraction separately in the DSC.

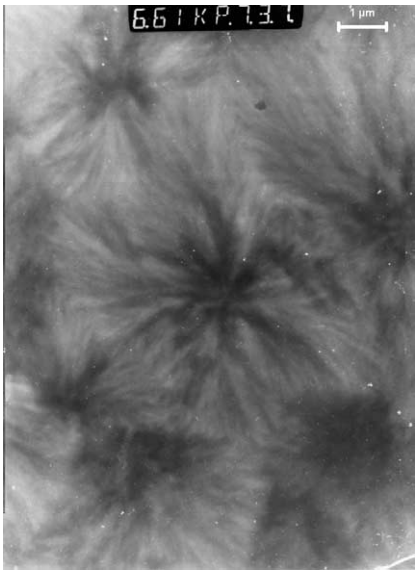

Fig. 12. TEM micrograph of PA6 cooled from the melt at the air.

3.3.2. The effect of the interface on droplet crystallization: variation in physical state of the matrix phase

Fig. 13 again shows the degree of fractionated crystallization as a function of the number of droplets for a number average and volume average droplet diameter. In these plots, however, the data for two PPE/PA6 blend compositions have been added. The weight fraction of PA6 these

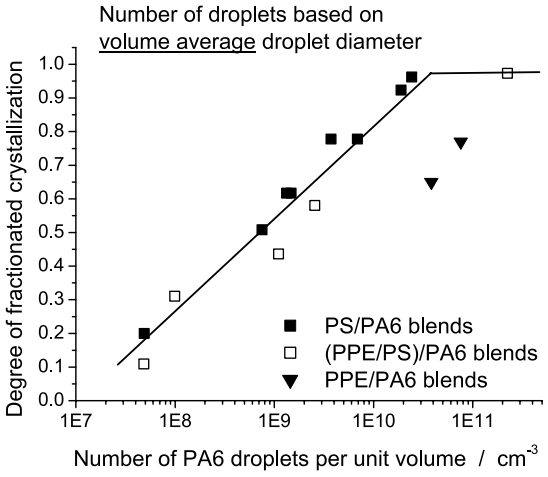

Fig. 13. Degree of fractionated crystallization for PS/PA6, (PPE/PS)/PA6 and PPE/PA6 blend compositions as a function of the number of droplets, calculated via the volume average droplet diameter.

blends was 10 and 15 wt% respectively, resulting in PA6 droplets of about 0.5 μm in diameter. The morphological and thermal data have been indicated in Table 3. The PPE component has much higher viscosity than both PS and (PPE/PS 50/50). These blend compositions show a significant lower degree of fractionated crystallization behavior than expected for the calculated number of droplets per unit volume. This effect does not disappear when plotting the number of droplets based on the volume average droplet diameter. Both blends show a relative low droplet size polydispersity. Apparently, the PPE/PA6 blends exhibit a higher nucleation density (of type 1 nuclei crystallizing at $T_{c,bulk}$), leading to a decrease in observed fractionated crystallization. Calculating the number of heterogeneities of type 1 via Eq. (9) using the volume average droplet diameter gives for M, the number of heterogeneities: 2×10^{11} nuclei/cm^3, more than a decade higher than the nucleation density for PS/PA6 and (PPE/PS)/PA6 blends (see above).

Migration of heterogeneities during melt-mixing from one component to the other could be a possible cause for the observed effect. The migration of heterogeneous nuclei during melt-mixing of immiscible blends is found to be critically depend on the mixing time of the blend components, the interfacial tension and the total interfacial area [38]. To induce the decrease of degree of fractionated crystallization as shown in Fig. 13 a considerable migration of heterogeneous nuclei from the PPE phase towards the PA6 should have occurred during melt mixing. All three blend systems, however, are mixed for the same time and exhibit equal interfacial tension. The total amount of interfacial area of the PPE/PA6 blend is comparable to the amount of interfacial area of the (PPE/PS)/PA6 85/15 blend. It thus seems unlikely that the PPE phase would induce a much stronger migration of heterogeneous nuclei towards PA6 than the PS and (PPE/PS) components.

An important difference between the PS, (PPE/PS)/PA6 and PPE/PA6 blends, however, is that the PPE phase has already vitrified before PA6 starts to crystallize whereas both PS and (PPE/PS) are still above their T_g when PA6 crystallization starts: T_g PPE = 215 °C > T_c PA6 188 °C. Everaert et al. [29] found similar changes in fractionated crystallization behavior for POM/(PPE/PS) blend compositions when the ratio PPE vs. PS was varied. An increased nucleation density of PA6 in these blends was found, leading to less fractionated crystallization, when the (PPE/PS) phase was solidified before the crystallization of POM started. The (PPE/PS) 50/50 component, with a T_g of about 150 °C solidifying before the bulk crystallization of POM at 145 °C, caused the nucleation density of POM to increase. The physical state of the matrix phase thus strongly influences the crystallization behavior of the dispersed droplets in the PPE/PA6 blends probably via nucleation of the PA6 phase promoted by the solid PPE surface. A possible explanation for this can be the change in surface tension of the PPE component on solidification, triggering nucleation. However, there seem to be no clear indications for a dramatic jump of surface tension upon passing the glass transition. The most probable explanation could be that it is caused by the different coefficients for thermal expansion of the matrix and the dispersed component, leading to pressure differences, inducing nucleation of the PA6 phase. This aspect needs further investigation to be solved completely.

4. Conclusions

In this report an overview of the fractionated crystallization phenomena is presented when PA6 is dispersed as small droplets within immiscible amorphous matrices of PS, (PPE/PS) and PPE. The results clearly confirm the strong competition between the number of dispersed PA6 droplets and the number of available nuclei causing fractionated

Table 3
Morphological and thermal properties of PPE/PA6 blend compositions

Sample	Wt% PA6	$D_{n,PA6}$ [μm]	P [−]	N_n [cm^{-3}]	$T_{c,peak}$ [°C]				Δh_c [J/g$_{PA6}$]			
					1	2	3	4	1	2	3	4
PA6	100	–	–	–	189	–	–	–	77	–	–	–
PPE/PA6	10	0.44	3.1	2.3×10^{12}	186	150	–	95	4	4	–	9
	15	0.58	3.4	1.5×10^{12}	187	150	–	90	8	5	–	10

crystallization. When the droplet size is small enough and the number of PA6 droplets exceeds the number of nuclei active at $T_{c,bulk}$, crystallization takes place in different steps, at larger degrees of supercooling, via nucleation by different types of nuclei that need a larger supercooling to become active. It is shown that the crystallization behavior of the droplets can be strongly affected by varying the thermal history of the sample. Self-nucleation experiments, giving rise to a strong increase in the number of nuclei crystallizing at $T_{c,bulk}$, can lead to a complete suppression of the fractionated crystallization phenomena. The physical state of the matrix phase is shown to be important too. When the amorphous phase is vitrified prior to crystallization, the nucleation densities increase, leading to much less fractionated crystallization in the dispersed droplets. The overall crystallization rate, measured after self-nucleation, decreases with decreasing PA6 droplet size (20–1 μm), indicating the disturbing effect of the small dimensions of the micrometer-sized PA6 droplets.

The degree of fractionated crystallization, characterized by the fraction of the droplets that crystallized at a temperature below $T_{c,bulk}$, can be fairly well related to the volume average droplet diameter. Assuming a Poisson distribution of heterogeneous nuclei over a droplet population with a volume average droplet size, the fractionated crystallization phenomenon can be used to give a quite reasonable estimation of the bulk heterogeneous nucleation density. The number of crystallization peaks below $T_{c,bulk}$, however, is shown to be very dependent on the droplet size distribution, leading to more peaks for broader distributions.

Acknowledgements

The authors are indebted to the Research Fund of the KULeuven (GOA 98/06), Belgium for the financial support given to the MSC-laboratory.

References

[1] Vonnegut B. J Colloid Sci 1948;3:563.
[2] Cormia RL, Price FP, Turnbull D. J Chem Phys 1962;37(6):1333.
[3] Burns JR, Turnbull D. J Appl Phys 1966;37(11):4021.
[4] Gornick F, Ross GS, Frolen LJ. Polym Prepr (Am Chem Soc Div Polym Chem) 1966;7:82.
[5] Koutsky JA, Walton AG, Baer E. J Appl Phys 1967;38(4):1832.
[6] Burns JR, Turnbull D. J Polym Sci Part A2 1968;6:775.
[7] Barham PJ, Jarvis DA, Keller A. J Polym Sci Phys Ed 1982;20:1733.
[8] Aref-Azar A, Hay JN, Marsden BJ, Walker N. J Polym Sci Phys Ed 1980;18:637.
[9] Ghysels A, Groesbeek N, Yip CW. Polymer 1982;23:1913.
[10] Klemmer N, Jungnickel BJ. Colloid Polym Sci 1984;262:381.
[11] Frensch H, Harnischfeger P, Jungnickel BJ. In: Utracki LA, Weiss RA, editors. Multiphase Polymers: Blends and Ionomers. ACS Symp Series, vol. 395, 1989. p. 101.
[12] Frensch H, Jungnickel BJ. Colloid Polym Sci 1989;267:16.
[13] Pukánszky B, Tüdös F, Kalló A, Bodor G. Polymer 1989;30:1399.
[14] Frensch H, Jungnickel BJ. Plastics. Rubber Compos Process Appl 1991;16:5.
[15] Baïtoul M, Saint-Guirons H, Xans P, Monge Ph. Eur Polym J 1991;17:1281.
[16] Avella M, Martuscelli E, Raimo M. Polymer 1993;34(15):3234.
[17] Ikkala OT, Holsti-Miettinen RM, Seppälä J. J Appl Polym Sci 1993;49:1165.
[18] Tang T, Huang B. J Appl Polym Sci 1994;53:355.
[19] Tang T, Huang B. J Polym Sci Part B: Polym Phys 1994;32:1991.
[20] Moon HS, Ryoo BK, Park JK. J Appl Polym Sci Part B, Polym Phys 1994;32:1427.
[21] Santana OO, Müller AJ. Polym Bull 1994;32(4):471.
[22] Morales RA, Arnal ML, Müller AJ. Polym Bull 1995;35(3):379.
[23] Manaure AC, Morales RA, Sánchez JJ, Müller AJ. J Appl Polym Sci 1997;66:2481.
[24] Molinuevo CH, Mendez GA, Müller AJ. J Appl Polym Sci 1998;70:1725.
[25] Arnal ML, Matos ME, Morales RA, Santana OO, Müller AJ. Macromol Chem Phys 1998;199(10):2275.
[26] Arnal ML, Müller AJ. Macromol Chem Phys 1999;200:2559.
[27] Arnal ML, Müller AJ, Maiti P, Hikosaka M. Macromol Chem Phys 2000;201(17):2493.
[28] Manaure AC, Müller AJ. Macromol Chem Phys 2000;201(9):958.
[29] Everaert V, Groeninckx G, Aerts L. Polymer 2000;41:1409.
[30] Psarski M, Pracella M, Galeski A. Polymer 2000;41:4923.
[31] Sanchez A, Rosales C, Laredo E, Muller AJ, Pracella M. Makromol Chem Phys 2001;202:2461.
[32] Groeninckx G, Vanneste M, Everaert V. In: Utracki LA, editor. Polymer Blends Handbook Polymer Blends Handbook. Crystallization, Morphological Structure and Melting of Polymer Blends, vol. 1. Dordrecht: Kluwer Academix Publishers; 2002. p. 203–94. Chapter 3.
[33] Wunderlich B. Macromolecular Physics. Crystal Nucleation-Growth-Annealing. vol. 2. New York/San Francisco/London: Academic Press; 1976.
[34] Price FP. J Amer Chem Soc 1952;74:311.
[35] Sharples A. Polymer 1962;3:250.
[36] Boon J, Challa G, Van Krevelen DW. J Polym Sci Part A2 1968;6:1835.
[37] Wenig W, Fiedel HW, Scholl A. Colloid Polym Sci 1990;268:528.
[38] Bartczak Z, Galeski A, Krasnikova NP. Polymer 1987;28:1627.
[39] Bartczak Z, Galeski A, Pracella M. Polymer 1986;27:537.
[40] Everaert V, Groeninckx G, Aerts L, Pionteck J, Favis BD, Moldenaers P, Mewis J. Polymer 1998;41:1011.
[41] Everaert V, Aerts L, Groeninckx G. Polymer 1999;40:6627.
[42] Blundell DJ, Keller A, Kovacs AJ. J Polym Sci 1966;B(4):481.
[43] Mathot VBF. Calorimetry and thermal analysis of polymers. The Crystallization and Melting Region. Munich/Vienna/New York: Carl Hanser Verlag; 1994. Chapter 9, p. 232–233.
[44] Fillon B, Wittmann JC, Lotz B, Thierry A. J Polym Sci Part B: Polym Phys 1993;31:1383.
[45] Fillon B, Lotz B, Thierry A, Wittmann JC. J Polym Sci: Part B: Polym Phys 1993;31:1395.
[46] Fillon B, Thierry A, Wittmann JC, Lotz B. J Polym Sci Part B; Polym Phys 1993;31:1407.
[47] Pound GM, LaMer VK. J Am Chem Soc 1952;74:2323.
[48] Tol RT, Groeninckx G, Vinckier I, Moldenaers P, Mewis J. Polymer 2004;45(8):2587–601.
[49] Dedecker K, Groeninckx G. Polymer 1998;39(21):4993.
[50] Billon N, Chanial L, Vivien B, Haudin JM. Ann Chim Fr 1995;20:355.
[51] Billon N, Haudin JM. Colloid Polym Sci 1989;267:1064.
[52] Tol RT, Mathot VBF, Reynaers H, Goderis B, Groeninckx G. Confined Crystallization Phenomena in Immiscible Polymer Blends with Dispersed Micro - and Nanometer Sized PA6 droplets. Part 4: Polymorphous structure and (meta)-stability of PA6 crystals formed in different temperature regions. Submitted to Polymer.